Title: **On robustness of optimal sensor placement to environmental variation for SHM**

Authors : Tingna Wang
David J. Wagg
Robert J. Barthorpe
Keith Worden

ABSTRACT

One challenge in establishing an effective structural health monitoring (SHM) system is the impact of environmental variability on damage identification. It is therefore, advantageous to consider any environmental effects when conducting sensor placement optimisation (SPO). One approach to this problem is to check the robustness of SPO technique to environmental variations and consider whether it is necessary to take account of these environmental factors as part of the optimisation process.

This paper will study the robustness of an SPO method to variations in the ambient temperature of the structure. Two kinds of data, including the mode shapes and the Mahalanobis squared-distance (MSD), from tests on a glider wing structure are used as features for SPO separately. This structure was set up and tested in different health states across a series of controlled temperatures. The results show that the SPO results obtained via the mode shapes are robust to the temperature variation, while the SPO results corresponding to MSD are sensitive to temperature changes.

INTRODUCTION

Sensor placement optimisation (SPO) is an essential technique by which a sensor system is optimised for a specific objective to provide an effective structural health monitoring (SHM) system. This process includes the selection of the number of sensors and the distribution of sensor spatial locations. The non-trivial step for this technique is to select an appropriate optimisation objective to evaluate the performance of a sensor system.

According to the type of data used in the SPO process, including the modal parameters, time-series data and frequency-domain data, SPO techniques and corresponding optimisation objectives can be discussed as follows. SPO techniques combined with modal parameters (such as natural frequency and the mode shape) have been developed to maximise the observability of the target modes [1], or the estimation accuracy of the target mode response [2]. SPO techniques combined with time-series data (such as the

Tingna Wang, David J. Wagg, Robert J. Barthorpe, Keith Worden, Dynamics Research Group, Department of Mechanical Engineering, University of Sheffield, Mappin Street, Sheffield, S1 3JD, UK. Email: twang71@sheffield.ac.uk
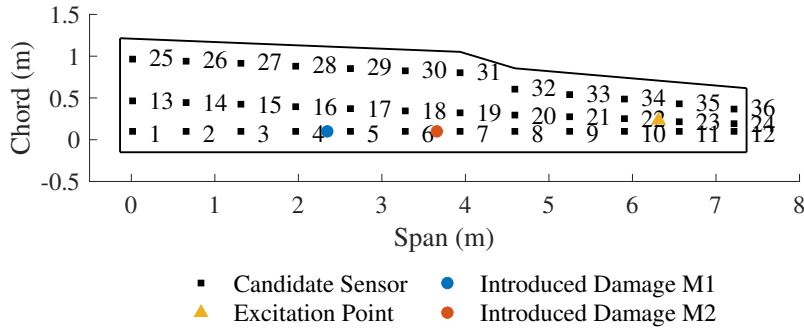
Figure 1. Labelled positions of significant points on the glider wing.

measured acceleration and strain) or frequency-domain data (such as the frequency response function (FRF) or the transmissibility function) have been developed to maximise the function of a statistical model [3, 4], or the accuracy of a structural parameter modification [5]. The robustness of optimal sensor placements obtained by two types of data, including mode shapes and FRFs, will be studied in this paper.

Because distinguishing the impact of damage from the impact of environmental changes is a major challenge in SHM, many studies in the literature have focussed on this issue [6–10]. Considering the availability of environmental variables, the approaches to dealing with the confounding effects can be divided into three types. When the measurements of environmental variables are accessible, the behaviours of the structure under each environmental condition can be explicitly modelled and the relationship between them can be established, as demonstrated by [6] and [8]. In contrast, some approaches, such as those developed by [7] and [9], can derive damage-sensitive features robust to environmental variations without using environmental measurements. In the case when the environmental measurements are partially available, how to make full use of data to eliminate environmental effects was discussed in [10].

In this paper, rather than exploring the SPO methods considering environmental effects, the necessity of taking account of environmental variations into the SPO process will be studied and discussed. The variation of one environmental parameter, temperature, is used as an example to specifically discuss its effect on the SPO results and an experiment on a glider wing is specially designed to provide suitable data sets.

The rest of the paper is organised as follows: Section 2 describes the experimental setup and collected data. Section 3 introduces two optimisation objectives and corresponding approaches to search out the optimal results. The results are discussed in Section 4, followed by the conclusions in Section 5.

EXPERIMENT SETUP AND DATA SET

A series of tests were performed on a glider wing to provide a data set suitable for this research. 36 candidate sensor locations are available as shown in Figure 1, which are drawn to scale. Damage is simulated by adding a mass block (60g) onto the structure. As demonstrated in Figure 1, two damage cases are considered: mass addition at locations M1 and M2.

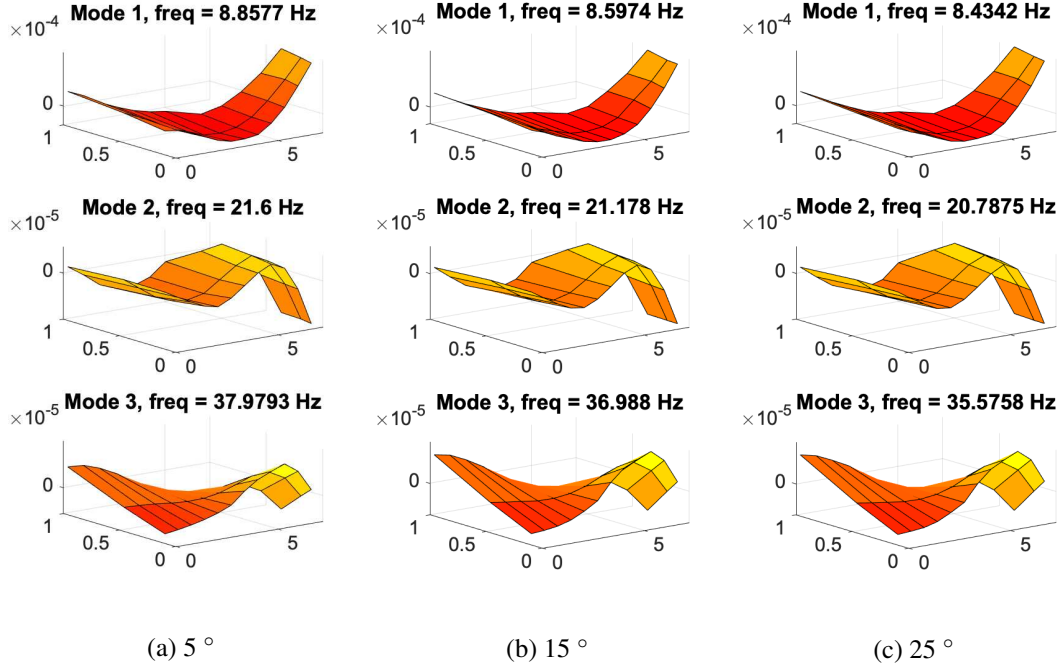| Mode 1, freq = 8.8577 Hz | Mode 1, freq = 8.5974 Hz | Mode 1, freq = 8.4342 Hz |
Mode 2, freq = 21.6 Hz	Mode 2, freq = 21.178 Hz	Mode 2, freq = 20.7875 Hz
Mode 3, freq = 37.9793 Hz	Mode 3, freq = 36.988 Hz	Mode 3, freq = 35.5758 Hz
(a) 5 °	(b) 15 °	(c) 25 °

Figure 2. The first three mode shapes of the glider wing.

A Gaussian white-noise excitation was generated and applied to the wing at a point between sensor 22 and sensor 23 using an ETS solutions VT100 electrodynamic shaker. FRFs were measured using PCB resonant piezoelectric accelerometers. The frequency range was 0-4096 Hz with frequency resolution 0.25 Hz. Six temperatures are considered: 0, 5, 10, 15, 20, 25 °C. At each temperature, one FRF, the average of 20 measurements, was measured firstly, followed by 25 'one-shot'-measurements of FRFs, and then another 20-averaged FRF.

Two types of data sets, including the mode shapes and the FRFs, were used to study the robustness of the optimal sensor placement. For the mode shape data set, the first three mode shapes were chosen and extracted from the 20-averaged FRFs to form the target mode matrix for each temperature. These mode shapes and corresponding natural frequencies at three different temperatures are shown in Figure 2.

For the FRF data set consisting of 25 single-averaged FRFs for each structural state at each temperature, the Mahalanobis squared-distance (MSD) was calculated for a selected frequency range to form a feature matrix, which can naturally eliminate the noise effect when all data have a similar noise level [11]. The adopted frequency range was 10 Hz to 50 Hz, covering the three natural frequencies corresponding to the three selected mode shapes. The equation to calculate MSD-based features is [12],

$$D_M^2 = (\mathbf{x} - \bar{\boldsymbol{\mu}})^\top \mathbf{S}^{-1} (\mathbf{x} - \bar{\boldsymbol{\mu}}) \tag{1}$$

where $\mathbf{x}$ is a vector referring to an observation, $\bar{\boldsymbol{\mu}}$ and $\mathbf{S}$ are the sample mean value and covariance matrix for a set of baseline observations respectively. $\top$ indicates transpose. A feature-bagging method is also used to avoid the singular covariance used in the MSD calculation by sampling spectral lines with repetition among a relatively-broad frequency range and averaging the features calculated from M sample data sets of spectral lines
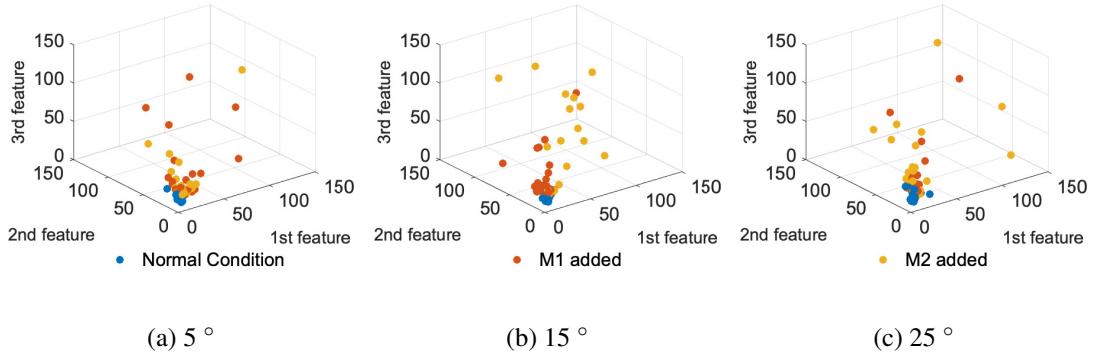
Figure 3. MSD-based features extracted from three sensors 5, 14 and 31

[11]. Features from three sensors 5, 14 and 31 collected at three temperatures are given as examples, as plotted in Figure 3.

OPTIMISATION TECHNIQUES

For the SPO using mode shapes as features, a trace-based criterion (introduced in Section 3.1) combined with an iterative technique is adopted to find a sub-optimal result under different temperatures. For the SPO using MSD-based features, another criterion based on the canonical correlation coefficient (CCC) is applied, which will be introduced in Section 3.2. A fast calculation approach for this criterion, combined with a greedy search is used to find the sub-optimal solution for different temperatures.

These two SPO technologies may sacrifice the performance of the designed sensor system to a certain extent, but they have higher computational efficiency. This means they are still practical when the size of search space is large, which is common in practice. In the following part, the word sub-optimal is replaced with optimal, keeping in mind the greedy nature of the algorithms.

Effective independence

One trace-based criterion used for the SPO based on mode shapes is referred to as *effective independence* (EI). Assume that there are limited candidate sensor locations and J modes to be identified. Suppose I sensors will be selected from the candidate sensors. For the sth combination of the I sensor locations, the outputs of these chosen sensors are described by a vector $\mathbf{y} \in R^{I \times 1}$, which is given by,

$$\mathbf{y}_s = \boldsymbol{\Phi}_s \mathbf{q}_s + \boldsymbol{\epsilon}_s \tag{2}$$

where $\boldsymbol{\Phi}_s \in R^{I \times J}$ is the sth target modal matrix, $\mathbf{q}_s \in R^{J \times 1}$ is the vector of the target modal coordinates and $\boldsymbol{\epsilon}_s \in R^{I \times 1}$ is the vector of measurement noise at these selected sensors, which is assumed to be zero-mean Gaussian noise and of equal variance σ^2. The least-squares estimation of the target modal coordinates for the sth sensor combination can be expressed as [1],

$$\hat{\mathbf{q}}_s = (\boldsymbol{\Phi}_s^\top \boldsymbol{\Phi}_s)^{-1} \boldsymbol{\Phi}_s^\top \mathbf{y}_s \tag{3}$$

The covariance matrix of the estimation error of the $\hat{\mathbf{q}}_\mathbf{s}$ is given by [1],

$$\mathbf{F}_{\hat{\mathbf{q}}_\mathbf{s}} = \sigma^2 (\mathbf{\Phi}_s^\top \mathbf{\Phi}_s)^{-1} \tag{4}$$

where $\mathbf{\Phi}_s^\top \mathbf{\Phi}_s$ is termed as the *Fisher information matrix* (FIM). According to the Gauss–Markov theorem [13], minimisation of this covariance matrix can help to obtain the best linear unbiased estimator of $\hat{\mathbf{q}}_s$. Referring to (4), it can be realised by maximising the FIM. Considering the contribution of each senor location, the FIM can be written as,

$$\mathbf{\Phi}_s^\top \mathbf{\Phi}_s = \sum_{i=1}^{I} \mathbf{\Phi}_s^{i\top} \mathbf{\Phi}_s^i \tag{5}$$

where $\mathbf{\Phi}_s^i$ is the ith row of the target modal matrix $\mathbf{\Phi}_s$ corresponding to the ith sensor location. It can be seen that each sensor location contributes some information to the FIM. In order to quantitatively evaluate the contribution of each location, the following eigenvalue equation can be solved,

$$(\mathbf{\Phi}_s^\top \mathbf{\Phi}_s - \lambda_s \mathbf{I}) \mathbf{\Psi}_s = \mathbf{0} \tag{6}$$

where $\mathbf{I}$ is an identity matrix. A relationship between the sensor locations and each eigenvalue can then be acquired by calculating the square of $\mathbf{\Phi}_s^i$ in terms of the basis formed by the columns $\mathbf{\Psi}_s$, which can be expressed as,

$$\mathbf{G} = (\mathbf{\Phi}_s \mathbf{\Psi}_s) \otimes (\mathbf{\Phi}_s \mathbf{\Psi}_s) \tag{7}$$

where the symbol $\otimes$ represents the element-wise product and the summation of jth column of $\mathbf{G}$ is equal to the jth eigenvalue of $\mathbf{\Phi}_s^\top \mathbf{\Phi}_s$. To make it possible to compare the contribution of each sensor location to the identification of J selected modes, the matrix $\mathbf{G}$ is right-multiplied by the inverse of the diagonal matrix $\boldsymbol{\lambda}_s = \mathbf{\Psi}_s^\top (\mathbf{\Phi}_s^\top \mathbf{\Phi}_s) \mathbf{\Psi}_s$ to rescale the columns, and then written as,

$$\mathbf{F_E} = (\mathbf{\Phi}_s \mathbf{\Psi}_s) \otimes (\mathbf{\Phi}_s \mathbf{\Psi}_s) \boldsymbol{\lambda}_s^{-1} \tag{8}$$

The sum of each column of $\mathbf{F_E}$ is equal to 1, which means that the contribution of one sensor location to identifying any selected mode can be quantitatively evaluated on the same scale, that is, within a range from 0 to 1. Thus, the sum of the ith row can be used to evaluate the contribution of the ith sensor location to the identification of J mode shapes.

On this basis, the vector composed of the sum of each row of $\mathbf{F_E}$ can be defined as the independence distribution vector $\mathbf{E_d}$, which can be formulated as the diagonal of an idempotent matrix,

$$\begin{aligned} \mathbf{E} &= \mathbf{\Phi}_s \mathbf{\Psi}_s \boldsymbol{\lambda}_s^{-1} \mathbf{\Psi}_s^\top \mathbf{\Phi}_s^\top \\ &= \mathbf{\Phi}_s (\mathbf{\Phi}_s^\top \mathbf{\Phi}_s)^{-1} \mathbf{\Phi}_s^\top \end{aligned} \tag{9}$$

where $\mathbf{E}$ is known as the projection matrix. Because the trace of an idempotent matrix is equal to its rank [14], the diagonal terms of the projection matrix $\mathbf{E}$ represent the contributions of the corresponding sensor locations to the linear independence of its columns or the mode shapes.

The values in the independence distribution vector $\mathbf{E_d}$ corresponding to sensor locations will be updated for each iteration of the SPO, which can indicate the importance of a sensor location to the independent information. Locations with small values in $\mathbf{E_d}$ can be removed at each iteration until a desired number of sensors are left. In this paper, only one sensor is removed at each iteration.

Furthermore, because sensor locations with low signal strength can be selected in the EI method, in this paper, the average driving-point residue (ADPR) is combined with the independence distribution vector $\mathbf{E_d}$ to overcome this issue by constructing the vector $\mathbf{E_d^{EI-DPR}}$ [15]. One entry in $\mathbf{E_d^{EI-DPR}}$ for the ith degree of freedom is given by,

$$E_{d_i}^{EI-DPR} = E_{d_i} \sum_{j=1}^{J} \frac{\phi_{ij}^2}{\omega_j} \tag{10}$$

where E_{d_i} is the ith entry in $\mathbf{E_d}$. ϕ_{ij} is the entry corresponding to the ith degree of freedom of the jth target mode in a target modal matrix. ω_j is the natural frequency corresponding to the jth target mode.

Sum of squared canonical correlation coefficients

For the features extracted from the frequency domain data, the objective function adopted here is based on the CCC; This coefficient is designed to measure the maximal linear association between a set of independent variables $\mathbf{X}$ and a set of other variables $\mathbf{Y}$ dependent on X [16]. It can be realised by finding L pairs of projection directions $\boldsymbol{\alpha}_l$ and $\boldsymbol{\beta}_l$, so that the Pearson's correlation coefficient between $\mathbf{X_C}\boldsymbol{\alpha}_l$ and $\mathbf{Y_C}\boldsymbol{\beta}_l$ is maximised, i.e.,

$$\begin{aligned} R(\mathbf{X}, \mathbf{Y}) &\triangleq \max_{\boldsymbol{\alpha}_l, \boldsymbol{\beta}_l} r(\mathbf{X}\boldsymbol{\alpha}_l, \mathbf{Y}\boldsymbol{\beta}_l) \\ &\triangleq \max_{\boldsymbol{\alpha}_l, \boldsymbol{\beta}_l} \frac{\boldsymbol{\alpha}_l^\top \mathbf{X}_\mathrm{C}^\top \mathbf{Y}_\mathrm{C} \boldsymbol{\beta}_l}{\sqrt{\boldsymbol{\alpha}_l^\top \mathbf{X}_\mathrm{C}^\top \mathbf{X}_\mathrm{C} \boldsymbol{\alpha}_l} \sqrt{\boldsymbol{\beta}_l^\top \mathbf{Y}_\mathrm{C}^\top \mathbf{Y}_\mathrm{C} \boldsymbol{\beta}_l}} \end{aligned} \tag{11}$$

where $\mathbf{X_C} = \mathbf{X} - \overline{\mathbf{X}}$ and $\mathbf{Y_C} = \mathbf{Y} - \overline{\mathbf{Y}}$. $\overline{\mathbf{X}}$ and $\overline{\mathbf{Y}}$ are the means of columns of $\mathbf{X}$ and $\mathbf{Y}$ respectively. $R(\cdot)$ refers to the CCC and $r(\cdot)$ refers to the Pearson's correlation coefficient. In this paper, a matrix $\mathbf{X} \in \mathbb{R}^{K \times N}$ represents the K observations with N independent features. A matrix $\mathbf{Y} \in \mathbb{R}^{K \times M}$ represents labels associated with each observation. If the $\mathbf{X}\boldsymbol{\alpha}_l$ and $\mathbf{Y}\boldsymbol{\beta}_l$ are standardised to have unit variance, (11) can be expressed as,

$$\max_{\boldsymbol{\alpha}_l, \boldsymbol{\beta}_l} \boldsymbol{\alpha}_l^\top \mathbf{X}_\mathrm{C}^\top \mathbf{Y}_\mathrm{C} \boldsymbol{\beta}_l, \quad \text{s.t. } \boldsymbol{\alpha}_l^\top \mathbf{X}_\mathrm{C}^\top \mathbf{X}_\mathrm{C} \boldsymbol{\alpha}_l = 1, \ \boldsymbol{\beta}_l^\top \mathbf{Y}_\mathrm{C}^\top \mathbf{Y}_\mathrm{C} \boldsymbol{\beta}_l = 1 \tag{12}$$

This equation is similar to (5) and the corresponding projection directions $\boldsymbol{\alpha}_l \in \mathbb{R}^{N \times 1}$ and $\boldsymbol{\beta}_l \in \mathbb{R}^{M \times 1}$ can be obtained by solving the eigenvalue equations given by [17],

$$\left[(\mathbf{X}_\mathrm{C}^\top \mathbf{X}_\mathrm{C})^{-1} \mathbf{X}_\mathrm{C}^\top \mathbf{Y}_\mathrm{C} (\mathbf{Y}_\mathrm{C}^\top \mathbf{Y}_\mathrm{C})^{-1} \mathbf{Y}_\mathrm{C}^\top \mathbf{X}_\mathrm{C} - \lambda_l \mathbf{I} \right] \boldsymbol{\alpha}_l = 0 \tag{13a}$$

$$\left[(\mathbf{Y}_\mathrm{C}^\top \mathbf{Y}_\mathrm{C})^{-1} \mathbf{Y}_\mathrm{C}^\top \mathbf{X}_\mathrm{C} (\mathbf{X}_\mathrm{C}^\top \mathbf{X}_\mathrm{C})^{-1} \mathbf{X}_\mathrm{C}^\top \mathbf{Y}_\mathrm{C} - \lambda_l \mathbf{I} \right] \boldsymbol{\beta}_l = 0 \tag{13b}$$

where the eigenvalue λ_l equals to the $R_l^2(\mathbf{X}, \mathbf{Y})$ and the maximum number of non-zero eigenvalues is not more than $\min(N, M)$, that is, L is not more than $\min(N, M)$.

On this basis, the sum of non-zero eigenvalues, i.e., the sum of squared canonical correlation coefficients (SSC), is adopted as a criterion for evaluating the effectiveness of a feature set from a sensor set to infer the structural state.

According to [18], the calculation speed of this criterion can be accelerated by the orthogonalisation of the feature matrix $\mathbf{X}_{\mathrm{C}}$ and the label matrix $\mathbf{Y}_{\mathrm{C}}$. Here, $\mathbf{W} \in \mathbb{R}^{K \times N}$ and $\mathbf{V} \in \mathbb{R}^{K \times M}$ are orthogonal bases for the column space of $\mathbf{X}_{\mathrm{C}}$ and the column space of $\mathbf{Y}_{\mathrm{C}}$ respectively. The SSC can be calculated by,

$$\sum_{l=1}^{\min(N, M)} R_l^2(\mathbf{X}, \mathbf{Y}) = \sum_{l=1}^{\min(N, M)} R_l^2(\mathbf{W}, \mathbf{V}) = \sum_{n=1}^{N}\sum_{m=1}^{M} r^2(\mathbf{w}_n, \mathbf{v}_m) \qquad (14)$$

where,

$$\mathbf{W} = (\mathbf{w}_1, \ldots, \mathbf{w}_N), \ \mathbf{V} = (\mathbf{v}_1, \ldots, \mathbf{v}_M)$$

By combining with a greedy search, the calculation of this criterion at each iteration is given by,

$$\sum_{l=1}^{\min((p+q), M)} R_l^2((\mathbf{X_s}, \mathbf{X_r}), \mathbf{Y}) = \sum_{l=1}^{\min(p, M)} R_l^2(\mathbf{W_s}, \mathbf{V}) + \sum_{l=1}^{\min(q, M)} R_l^2(\mathbf{W_r}, \mathbf{V}) \qquad (15)$$

where $\mathbf{X_s}$ is composed of the p selected features in the previous steps and $\mathbf{X_r}$ represents the features to be selected at the current step. $\mathbf{W_s} \in \mathbb{R}^{K \times p}$ and $\mathbf{W_r} \in \mathbb{R}^{K \times q}$ are orthogonal bases for the column space of $\mathbf{X_s}$ and the column space of $\mathbf{X_r}$ respectively. $\mathbf{W_r}$ is orthogonal to $\mathbf{W_s}$.

The iterative calculation is also applied in this part but one sensor is added rather than reduced at each iteration of a greedy search, i.e., $q = 1$ in (15). Thus, the matrix $\mathbf{W_r} \in \mathbb{R}^{K \times q}$ in (15) degenerates to the vector $\mathbf{w_r} \in \mathbb{R}^{K \times 1}$ and $\mathbf{w_r}$ is orthogonal to $\mathbf{W_s}$. At each iteration, the sensor which can provide a feature to maximise $R_l^2(\mathbf{w_r}, \mathbf{V})$ will be selected until the required number of sensors is reached.

Note that the labels can usually be represented by a vector, i.e., $M = 1$. In this situation, the applied criterion reduces to the squared multiple correlation coefficient $R^2(\mathbf{X}, \mathbf{y})$. However, $M > 1$ may happen, for example, when the responses are multi-class categorical labels, which do not have an inherent order. This is the situation in this paper. These labels can be dummy encoded to a matrix $\mathbf{Y}$, in which each category is transformed into a set of binary variables to use M variables to represent $(M + 1)$ categories. One advantage of the dummy encoding is that it can make the label matrix $\mathbf{Y}$ remain full column rank after subtracting its column mean.

RESULTS AND DISCUSSION

Three to ten sensors are selected in all cases. The optimal results for the SPO based on mode shapes are shown in Figure 4. It can be seen that the obtained sensor distributions with a fixed number of sensors always contain the same sensor at all controlled temperatures. When considering all the optimal sensor distributions, two sensors, including sensors 10 and 36, will always be selected at all temperatures.

The signal strength is then taken into account in the optimisation process by using the modified distribution vector $\mathbf{E_d^{EI-DPR}}$. The optimal results are visualised in Figure
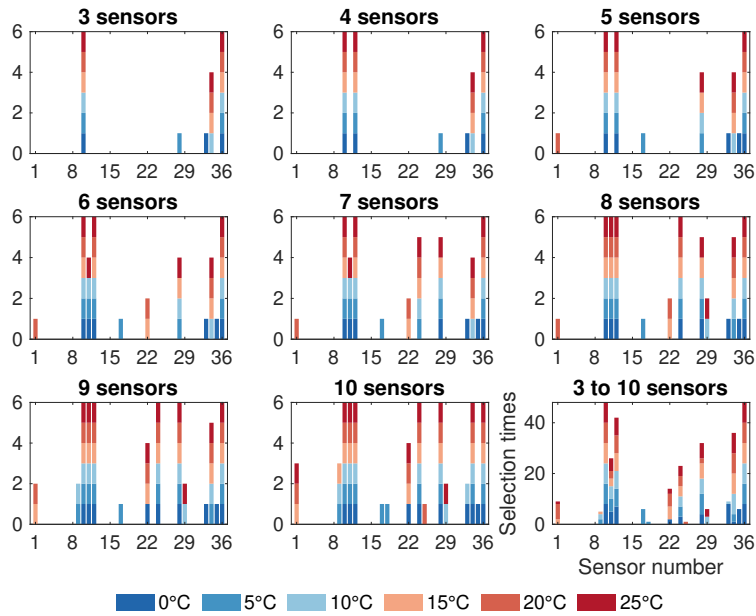
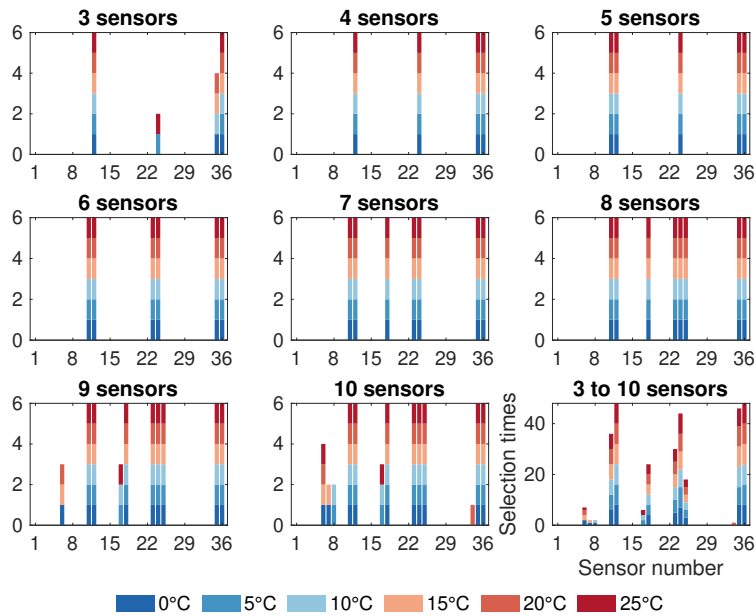Figure 4. Histogram of the EI-based optimal sensor distributions.

Figure 5. Histogram of the EI-DPR-based optimal sensor distributions.

5. It was found that there is a significant increase in the number of the same sensors contained in the optimal sensor distributions corresponding to different temperatures. When considering all the optimal sensor distributions, although there are still two sensors (12 and 36) selected at all temperatures, the total number of selected sensors decreases from 16 to 13.

Compared with the EI optimisation results, the results corresponding to EI-DRP are more robust to temperature variations. This phenomenon is reasonable considering the effect of the signal-to-noise ratio. A sensor combination composed of sensors with a low
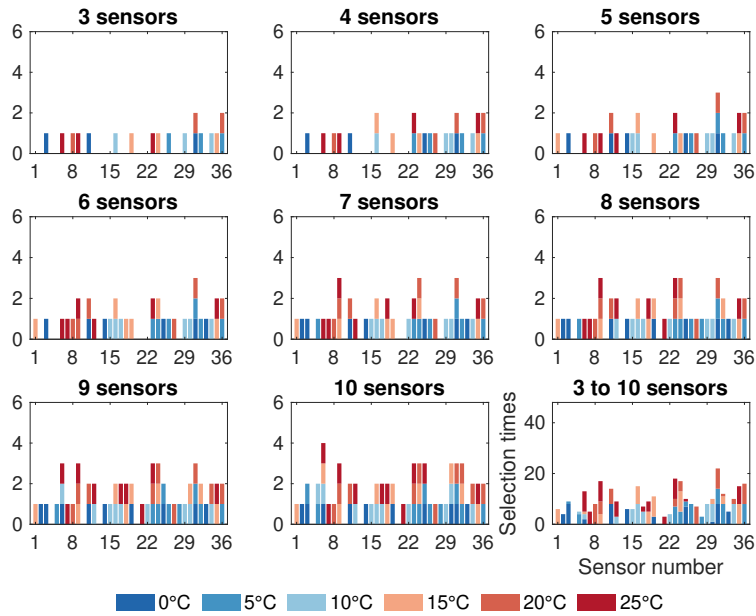
Figure 6. Histogram of the SSC-based optimal sensor distributions for M1 detection.
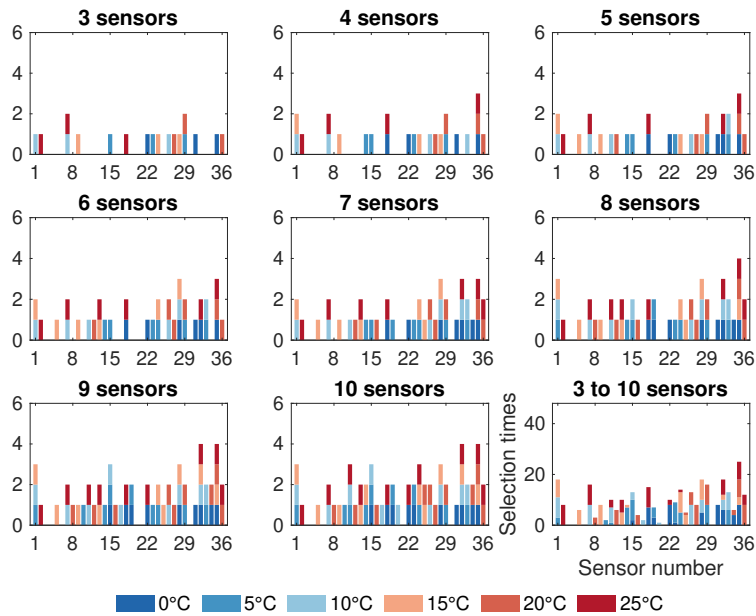

Figure 7. Histogram of the SSC-based optimal sensor distributions for M1M2 detection.

signal-to-noise ratio can provide a modal data set that is more robust to the changes of temperature. In summary, it is acceptable to ignore the temperature factor in the SPO based on the mode shapes, especially for the case with the signal strength considered.

The optimal results of the MSD-based SPO designed for M1 detection are shown in Figure 6. The results optimised for the detection of M1 and M2 are shown in Figure 7. When considering all the optimal sensor distributions with the number of sensors from three to ten, there are 32 and 31 sensors contained in these optimal distributions designed for the two mentioned tasks respectively. The number of the sensors contained

in these optimal results is obviously larger that that obtained by the SPO based on the mode shapes. Furthermore, no sensor is always selected at all temperatures for any cases. Therefore, for the SPO with MSD-based features, the temperature effect should obviously be considered in the optimisation process.

CONCLUSIONS

This paper analyses the robustness of two SPO techniques to environmental variations, to illustrate the effect of an environmental parameter in the optimisation process. Two commonly-used data types are considered, i.e., mode shapes and MSD-based features; the entire process is demonstrated in detail with temperature as an example.

Data of a glider wing collected at different temperatures are used for a case study. Mode shapes are combined with EI and EI-DRP technologies to optimise the sensor combinations for modal identification. In addition, MSD-based features are combined with a greedy search to optimise the sensor deployments for damage identification. A fast calculation of the optimisation objective, SSC, is adopted to speed up the calculation.

The results mainly show that the modal features from the candidate sensors have a more consistent relationship at different temperatures, especially when the signal amplitude is considered. Hence, the participation of temperature is avoidable for the SPO based on mode shapes. In contrast, the relationship of MSD features for different structural states is greatly affected by temperature. Therefore, SPO using MSD-based features inevitably must take this environmental factor into consideration.

REFERENCES

1. Kammer, D. C. 1991. "Sensor placement for on-orbit modal identification and correlation of large space structures," *J GUID CONTROL DYNAM*, 14(2):251–259.
2. Yao, L., W. A. Sethares, and D. C. Kammer. 1993. "Sensor placement for on-orbit modal identification via a genetic algorithm," *AIAA J*, 31(10):1922–1928.
3. Krause, A., A. Singh, and C. Guestrin. 2008. "Near-optimal sensor placements in Gaussian processes: Theory, efficient algorithms and empirical studies." *J MACH LEARN RES*, 9(8):235–284.
4. Worden, K., G. Manson, G. Hilson, and S. Pierce. 2008. "Genetic optimisation of a neural damage locator," *J SOUND VIB*, 309(3-5):529–544.
5. Papadimitriou, C. 2004. "Optimal sensor placement methodology for parametric identification of structural systems," *J SOUND VIB*, 278(4-5):923–947.
6. Farrar, C. R., H. Sohn, and K. Worden. 2001. "Data normalization: a key for structural health monitoring," Tech. rep., Los Alamos National Lab., New Mexico, United States.
7. Cross, E., G. Manson, K. Worden, and S. Pierce. 2012. "Features for damage detection with insensitivity to environmental and operational variations," *P ROY SOC A-MATH PHY*, 468(2148):4098–4122.
8. Worden, K., E. J. Cross, and J. M. Brownjohn. 2013. "Switching response surface models for structural health monitoring of bridges," in *Surrogate-Based Modeling and Optimization*, Springer, pp. 337–358.
9. Deraemaeker, A. and K. Worden. 2018. "A comparison of linear approaches to filter out environmental effects in structural health monitoring," *MECH SYST SIGNAL PR*, 105:1–15.

10. Liu, A., L. Wang, L. Bornn, and C. Farrar. 2019. "Robust structural health monitoring under environmental and operational uncertainty with switching state-space autoregressive models," *STRUCT HLTH MONIT*, 18(2):435–453.

11. Bull, L., K. Worden, R. Fuentes, G. Manson, E. Cross, and N. Dervilis. 2019. "Outlier ensembles: A robust method for damage detection and unsupervised feature extraction from high-dimensional data," *J SOUND VIB*, 453:126–150.

12. Barnett, V. and T. Lewis. 1984. *Outliers in Statistical Data (2th ed.)*, John Wiley & Sons, Chichester, United Kingdom.

13. Henderson, C. R. 1975. "Best linear unbiased estimation and prediction under a selection model," *Biometrics*:423–447.

14. Greene, W. H. 2003. *Econometric Analysis (5th ed.)*, Pearson Education, Inc., New Jersey, United States.

15. Imamovic, N. 1998. *Validation of Large Structural Dynamics Models Using Modal Test Data*, Ph.D. thesis, Imperial College London.

16. Hotelling, H. 1936. "Relations between two sets of variates," *Biometrika*, 28(3/4):321–377.

17. Hardoon, D. R., S. Szedmak, and J. Shawe-Taylor. 2004. "Canonical correlation analysis: An overview with application to learning methods," *Neural Comput.*, 16(12):2639–2664.

18. Zhang, S., T. Wang, K. Worden, and E. J. Cross. 2021. "Canonical-correlation-based fast feature selection," *arXiv preprint arXiv:2106.08247*.